Received: 27 June 2023 | Revised: 30 August 2023 | Accepted: 19 September 2023

DOI: 10.1002/nbm.5058

RESEARCH ARTICLE

NMR IN BIOMEDICINE WILEY

Rotator cuff muscle fibrosis can be assessed using ultrashort echo time magnetization transfer MRI with fat suppression

Eric Y. Chang[1,2] | Arya Suprana[2,3] | Qingbo Tang[2,4] | Xin Cheng[2,4] | Eddie Fu[2,4] | Elisabeth Orozco[4,5] | Saeed Jerban[2,4,5] | Sameer B. Shah[3,4,5] | Jiang Du[2,3,4] | Yajun Ma[2,4]

[1]Radiology Service, VA San Diego Healthcare System, San Diego, California, USA

[2]Department of Radiology, University of California San Diego, San Diego, California, USA

[3]Department of Bioengineering, University of California San Diego, San Diego, California, USA

[4]Research Service, VA San Diego Healthcare System, San Diego, California, USA

[5]Department of Orthopedic Surgery, University of California San Diego, San Diego, California, USA

Correspondence
Eric Y. Chang, Radiology Service, VA San Diego Healthcare System, 3350 La Jolla Village Drive, San Diego, CA 92161, USA.
Email: ericchangmd@gmail.com

Funding information
U.S. Department of Veterans Affairs, Grant/Award Numbers: I01CX001388, I01BX005952, I01CX000625; National Institutes of Health, Grant/Award Numbers: R01AR068987, R01AR062581, R01AR075825, K01AR080257, R01AR079484, R21AR075851

Abstract

Muscle degeneration following rotator cuff tendon tearing is characterized by fatty infiltration and fibrosis. While tools exist for the characterization of fat, the ability to noninvasively assess muscle fibrosis is limited. The purpose of this study was to evaluate the capability of quantitative ultrashort echo time T1 (UTE-T1) and UTE magnetization transfer (UTE-MT) mapping with and without fat suppression (FS) for the differentiation of injured and control rotator cuff muscles and for the detection of fibrosis. A rat model of chronic massive rotator cuff tearing ($n = 12$) was used with tenotomy of the right supraspinatus and infraspinatus tendons and silicone implants to prevent healing. Imaging was performed on a 3-T scanner, and UTE-T1 mapping with and without FS and UTE-MT with and without FS for macromolecular fraction (MMF) mapping was performed. At 20 weeks postinjury, T1 and MMF were measured in the supraspinatus and infraspinatus muscles of the injured and contralateral, internal control sides. Histology was performed and connective tissue fraction (CTF) was measured, defined as the area of collagen-rich extracellular matrix divided by the total muscle area. Paired *t*-tests and correlation analyses were performed. Significant differences between injured and control sides were found for CTF in the supraspinatus (mean ± SD, 14.5% ± 3.9% vs. 11.3% ± 3.7%, $p = 0.01$) and infraspinatus (17.0% ± 5.4% vs. 12.5% ± 4.6%, $p < 0.01$) muscles, as well as for MMF using UTE-MT FS in the supraspinatus (9.7% ± 0.3% vs. 9.5% ± 0.2%, $p = 0.04$) and infraspinatus (10.9% ± 0.8% vs. 10.1% ± 0.5%, $p < 0.01$) muscles. No significant differences between sides were evident for T1 without or with FS or for MMF using UTE-MT. Only MMF using UTE-MT FS was significantly correlated with CTF for both supraspinatus ($r = 0.46$, $p = 0.03$) and infraspinatus ($r = 0.51$, $p = 0.01$) muscles. Fibrosis occurs in rotator cuff muscle degeneration, and the UTE-MT FS technique may be helpful to evaluate the fibrosis component, independent from the fatty infiltration process.

Abbreviations: CSA, cross-sectional area; CTF, connective tissue fraction; FA, flip angle; FS, fat suppression; H&E, hematoxylin and eosin; ICC, intraclass correlation; MMF, macromolecular fraction; MRI, magnetic resonance imaging; MSK, musculoskeletal; MT, magnetization transfer; OCT, optimal cutting temperature; PDMS, polydimethylsiloxane; PFA, paraformaldehyde; RARE, rapid imaging with refocused echoes; ROI, region of interest; STEAM-FLASH, stimulated echo acquisition mode-fast low angle shot; TE, echo time; TR, repetition time; UTE, ultrashort echo time; UTE-MT, ultrashort echo time magnetization transfer; UTE-T1, ultrashort echo time T1.

KEYWORDS
fibrosis, magnetization transfer, rotator cuff muscle, ultrashort TE

1 | INTRODUCTION

The rotator cuff is the primary stabilizer of the glenohumeral joint and disruption leads to abnormal joint kinematics, deterioration of function, and progression towards osteoarthritis.[1] Surgical repair may be an option after rotator cuff tendon tearing, but successful reduction of the torn tendon and subsequent clinical outcome depend, to a large extent, on the status of the muscle.[2,3] Muscle degeneration following rotator cuff tendon tearing, characterized by fatty infiltration and fibrosis, potentially increases the retear rates by up to 94% after technically successful repairs.[4–6]

In clinical practice, magnetic resonance imaging (MRI) is the reference standard for the assessment of muscle quality after rotator cuff tendon tearing, but the evaluation is primarily qualitative and limited to descriptions of the degree of atrophy and fatty infiltration.[7] Quantitative MRI, in particular T1 (spin–lattice) relaxation time, has been investigated as a potential tool for the evaluation of muscle, but the measurements are believed to primarily reflect fat content.[8–12] Magnetization transfer (MT) measures, which provide information on the macromolecular and free water pools, have also been used on muscles.[13–19] However, the specificity of the MT measurements is unclear because some have shown significant correlations with intramuscular fat[19] and others have shown significant correlations with protein concentrations.[15] Fat suppression (FS) techniques have been suggested by some authors to disambiguate measurements of the macromolecular pool in the presence of fatty infiltration.[17,20] Transverse relaxation time (spin–spin) has been used on rotator cuff muscles as well,[21] but T2 measurements are mostly sensitive to edema and inflammatory changes.[22]

Recently, ultrashort echo time (UTE)-MT imaging with two-pool modeling has been applied to the rotator cuff tendons, demonstrating a strong correlation with collagen content.[23] The UTE acquisition permits high signal evaluation of the short T2 regions, including tendon and fibrotic regions. At present, there are limited tools available to assess muscle fibrosis noninvasively. Although T1 and MT measures with FS have been suggested for this purpose,[17,20] these tools have not been rigorously evaluated, nor have the techniques been used for the rotator cuff musculature. The purpose of this study was to evaluate the capability of quantitative UTE-T1 and UTE-MT mapping with and without FS for the differentiation of injured and control rotator cuff muscles and for the detection of fibrosis in a rat model of chronic massive rotator cuff tearing. We hypothesized that quantitative UTE imaging with FS would be able to differentiate between the injured and control sides, and could be used to detect fibrosis in the degenerated rotator cuff muscles.

2 | METHODS

2.1 | Rat rotator cuff tear model

Our experiment was approved by the VA San Diego Healthcare System Institutional Animal Care and Use Committee. A rat model of chronic massive rotator cuff tearing was adapted, which is known to induce muscle collagen deposition and fatty infiltration as early as 4 weeks postoperatively.[24] Twelve 13-week-old Lewis rats were used. Anesthesia was induced with 4% isoflurane and maintained for the duration of the surgery at 1%–2%. Thermoregulation was achieved using an aqua thermal pad, and heart rate and respiratory rate were monitored throughout the surgery. Surgeries were performed on the right shoulder and the unoperated left shoulder was used for paired comparisons. Right supraspinatus and infraspinatus tenotomies were performed and the distal 2–3 mm of the tendons were removed. A thin, L-shaped silicone (polydimethylsiloxane [PDMS]) implant was placed over the greater tuberosity and firmly fixed with a size 2-0 nonabsorbable polyester suture to prevent spontaneous tendon healing. Overlying deltoid muscle and skin were closed, and the rats were allowed unrestricted cage activity.

2.2 | MRI

All imaging was performed on a 3-T MRI scanner (Bruker BioSpec 3-T, Billerica, MA, USA) using an 82 mm volume coil for transmission and a 30 mm surface coil for reception. Anesthesia was induced with 5% isoflurane and maintained for the duration of the imaging at 1%–1.5%. At 5-, 8-, 13-, and 20 weeks postinjury, a conventional MRI protocol was employed consisting of T1-weighted and fluid-sensitive sequences, which are the most commonly used sequences in clinical practice for rotator cuff and muscle evaluation.[25]

Specifically, axial oblique T1-weighted (repetition time/echo time [TR/TE] = 522/13 ms) nonfat-suppressed and T2-weighted (TR/TE = 2022/60 ms) with chemical FS rapid imaging with refocused echoes (RARE) sequences were used on both shoulders of each rat at 5 cm

field of view, 256 × 256 matrix, and 2 mm slice thickness (0.2 × 0.2 × 2 mm resolution). Twelve slices were acquired per sequence. As the rat scapulae are obliquely oriented with more upward rotation compared with humans, an axial oblique imaging plane yields imaging sections similar to sagittal-oblique images in humans.

At 20 weeks postinjury, an additional quantitative imaging protocol was performed, consisting of 3D UTE-T1 mapping with and without chemical shift FS (TR/TE = 12/0.026 ms, flip angles [FAs] = 4/8/12/16°, 0.5 mm isotropic resolution, scan time ~5 min per acquisition), 3D UTE-MT mapping with and without chemical shift FS (MT preparation using a Fermi-shaped pulse with 500/1500° FAs and frequency offsets of 2/5/10/20/50 kHz, TR/TE = 62/0.026 ms, spoke interval = 4 ms, number of spokes per-TR = 10, FA = 7°, 0.5 mm isotropic resolution, scan time ~3 min per acquisition), and a vendor-provided stimulated echo acquisition mode-fast low angle shot (STEAM-FLASH) sequence for B1 correction in both T1 estimation and MT modeling (STEAM FA = 60°, TR/TE = 2000/2.2 ms, FA = 15°, 1.6 × 1.6 × 4.2 mm resolution, averages = 15, scan time ~4 min).

In five arbitrarily selected rats, postmortem imaging was performed using a high-resolution intermediate-weighted 3D RARE sequence (TR/TE = 1500/30 ms, RARE factor = 6, 0.3 mm isotropic resolution, averages = 7, scan time ~9 h per rat).

2.3 | Magnetic resonance image analysis

Analysis was performed on the image closest to the glenohumeral joint where the scapular spine was in contact with the scapular body, similar to that used in routine clinical practice.[26] A fellowship-trained, board-certified musculoskeletal (MSK) radiologist with 12 years of experience (E.Y.C.) evaluated the T2-weighed FS images for the presence of rotator cuff muscular edema throughout all the timepoints, defined as increased signal in the belly relative to surrounding, noninjured muscles, excluding fascia. In addition, the MSK radiologist measured the cross-sectional areas (CSAs) of the muscles, generated a ratio of the CSAs of the injured/uninjured sides, and applied the Goutallier classification[27] on the RARE images, using RadiAnt DICOM Viewer (v. 2020.2.3, Medixant, Poznan, Poland). After 6 months of training by the MSK radiologist to identify the anatomy and muscle boundaries, a Ph.D. student (A.S.) independently drew regions of interest (ROIs) around the muscles on a single reconstructed UTE-MT non-FS image with RARE images as an extra guide. A single ROI was used for each muscle. The ROIs were propagated to all UTE sequences for calculation of T1 and macromolecular fraction (MMF) values from two-pool modeling on a pixel-by-pixel basis using MATLAB (MathWorks, Natick, MA, USA). A Levenberg–Marquardt algorithm was employed for the nonlinear least-squares fitting for T1 fitting as well as for the MT model. Two-pool UTE-MT modeling and parameter mapping were performed on the datasets as previously described,[28] including T1 correction with the respective FS condition (i.e., modeling of UTE-MT with FS data included the measured T1 from the UTE-T1 with FS sequence). Pixel values within the ROI were averaged. To assess interobserver reliability, 12 rotator cuff muscles were randomly selected and the MSK radiologist repeated the UTE quantification. The radiologist and Ph.D. student were blinded to the other's quantification results.

2.4 | Histological preparation and analysis

At 20 weeks postinjury, the rats were perfused transcardially with 4% paraformaldehyde (PFA) in phosphate buffer. The scapula and proximal humeri were resected en bloc, postfixed in PFA at 4°C for 48 h, then transferred to a solution of 20% ethylenediaminetetraacetic acid for 4 weeks at room temperature for decalcification. The medium was changed every 72 h and decalcification was checked by radiography at weekly intervals. Following decalcification, the samples were copiously washed in saline, treated with 30% sucrose for cryoprotection, snap-frozen in liquid nitrogen-cooled isopentane, then embedded in optimal cutting temperature (OCT) compound. Twelve micrometer-thick cryosections were made in the transverse direction relative to the spine and body of the scapula, targeting the same location as the MRI (where the scapular spine was in contact with the scapular body). Sections were stained with hematoxylin and eosin (H&E) and Masson trichrome (Epredia Richard-Allan Scientific Masson Trichrome Kit, 22110648, Fisher Scientific, Hampton, NH, USA). Slides were digitized using a slide scanner (AxioScan Z1, ZEISS, Thornwood, NY, USA) with a 20× objective.

Cell diameter and perimeter were calculated in the transverse sections of 60 randomly selected myofibers for each muscle. In addition, connective tissue fraction (CTF) was calculated, defined as the area of collagen-rich extracellular matrix (stained blue with Masson trichrome) divided by the total muscle area, similar to previous methodology.[29] Histologic quantification was performed by a blinded pathologist with 23 years of experience (X.C.) using computer-assisted image analysis software (HALO, Indica Labs, Albuquerque, NM, USA).

2.5 | Statistical analysis

A power analysis estimated a required sample size of 11 to detect an effect size of 1.0 (determined based on histologic muscle data from previous studies of chronic massive rotator cuff tears[30–32]), with 80% power and significance level set to 0.05. The Shapiro–Wilk test was used to assess

data normality distribution and the appropriate statistical test was chosen based on the data. Descriptive statistics were performed. Paired *t*-tests were used to evaluate the differences in the groups. Relationships were assessed using Spearman's and Pearson's correlation as appropriate. Two-way mixed intraclass correlation (ICC) coefficients were used to assess interobserver reliability for UTE quantification and interpreted as follows: less than 0.50 as poor, between 0.50 and 0.75 as moderate, between 0.75 and 0.90 as good, and greater than 0.90 as excellent.[33] p less than 0.05 was considered to represent significant findings. Statistical analysis was performed using the SPSS software package (version 21; SPSS, Chicago, IL, USA).

3 | RESULTS

3.1 | Rat rotator cuff tear model

Figure 1 demonstrates the chronic massive rotator cuff tear model using the silicone implant. Intramuscular edema was present in all injured supraspinatus and infraspinatus muscles at 5, 8, and 13 weeks, although an improvement was evident in all rats at later timepoints compared with earlier timepoints. At 20 weeks postinjury, nine of the 12 rats (75%) remained with subtle, but detectable edema within the injured muscles, although all decreased compared with prior timepoints (Figure 2).

3.2 | Morphological analysis of conventional MRI

As measured on T1-weighted images, Goutallier grades were significantly higher for the injured sides compared with the control sides for both the supraspinatus (mean ± SD, 1.0 ± 0.6 vs. 0.0 ± 0.0, $p < 0.01$) and infraspinatus (1.8 ± 0.8 vs. 0.3 ± 0.5, $p < 0.01$) muscles (Figures 2 and 3). CSA measurements were significantly smaller for the injured sides compared with the control sides for both the supraspinatus (mean ± SD, 23.3 ± 5.9 vs. 35.4 ± 7.7 mm^2, $p < 0.01$) and infraspinatus (16.5 ± 4.8 vs. 27.5 ± 7.1 mm^2, $p < 0.01$) muscles.

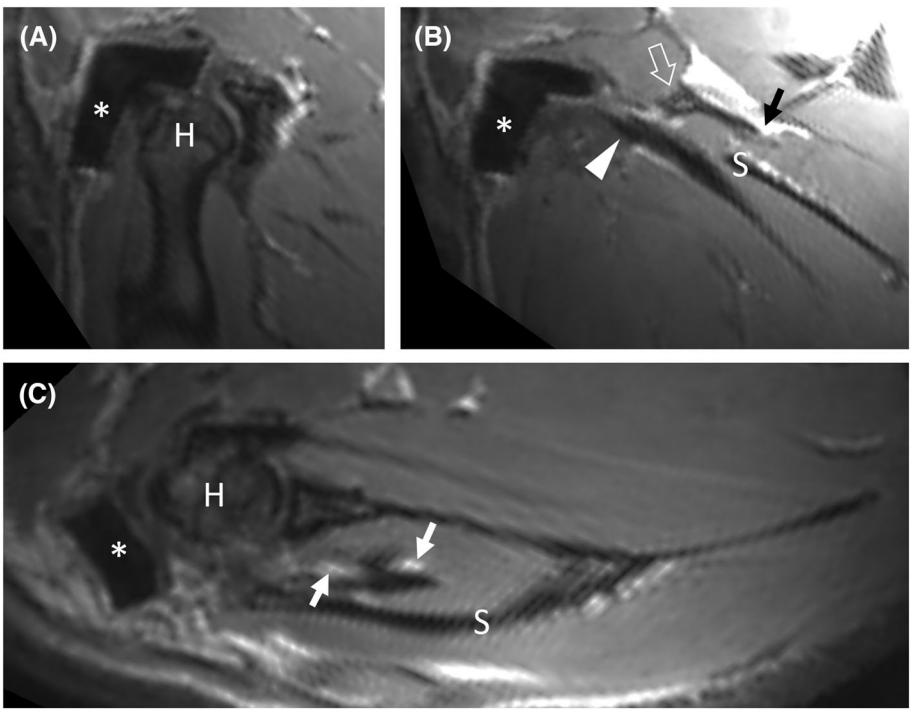

FIGURE 1 Rat chronic massive rotator cuff tear model. Reformatted 3D rapid imaging with refocused echoes (3D RARE) images through the right shoulder of a rat at 20 weeks postinjury, in planes equivalent to the coronal oblique (A and B) and axial oblique (C) planes in humans. The silicone implant (asterisk) covers the greater tuberosity of the proximal humerus. The torn and retracted margins of the supraspinatus (open arrow) and infraspinatus (arrowhead) tendons are shown in (B). Peritendinous fatty infiltration is present in the supraspinatus (B, black arrow) and infraspinatus (C, arrows) myotendinous regions. Stripe artifacts in the images are due to the multiplanar reconstruction. H, humerus; S, scapular spine.

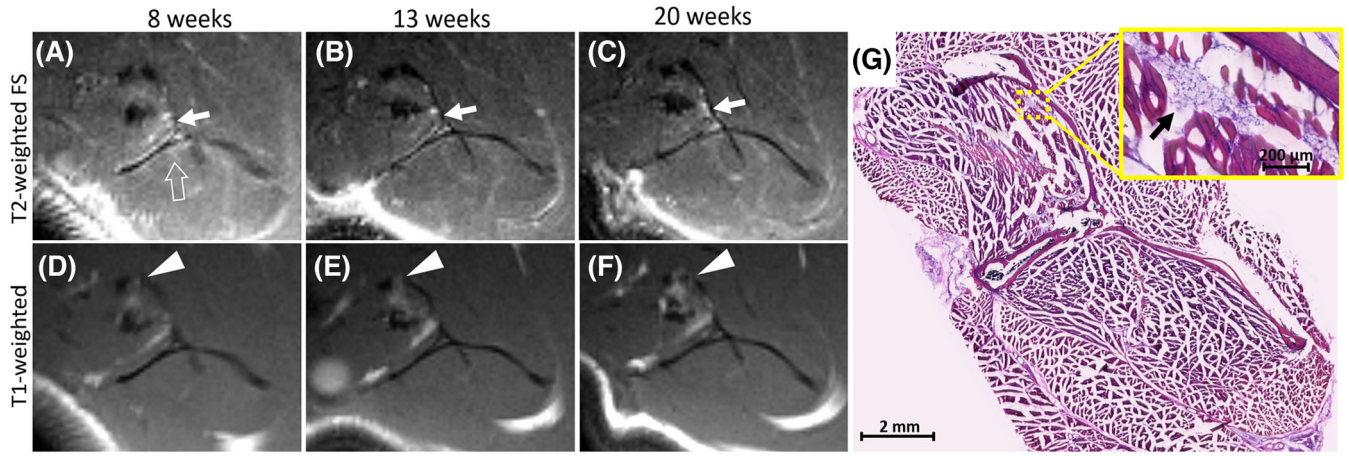

FIGURE 2 Representative longitudinal muscle changes postinjury. Transverse T2-weighted fat-suppressed (A–C) and T1-weighted (D–F) rapid imaging with refocused echoes (RARE) images at (A and D) 8, (B and E) 13, and (C and F) 20 weeks postinjury. Edema is present in the infraspinatus (arrows) and supraspinatus (open arrow) muscles, improving at later timepoints, although it is still evident in the infraspinatus at 20 weeks. Fatty infiltration is also evident in the infraspinatus (arrowheads), with Goutallier grade 3 at 20 weeks. On the hematoxylin and eosin (H&E) image (G), architectural distortion is evident in the infraspinatus muscle with abundant adipocytes (inset image).

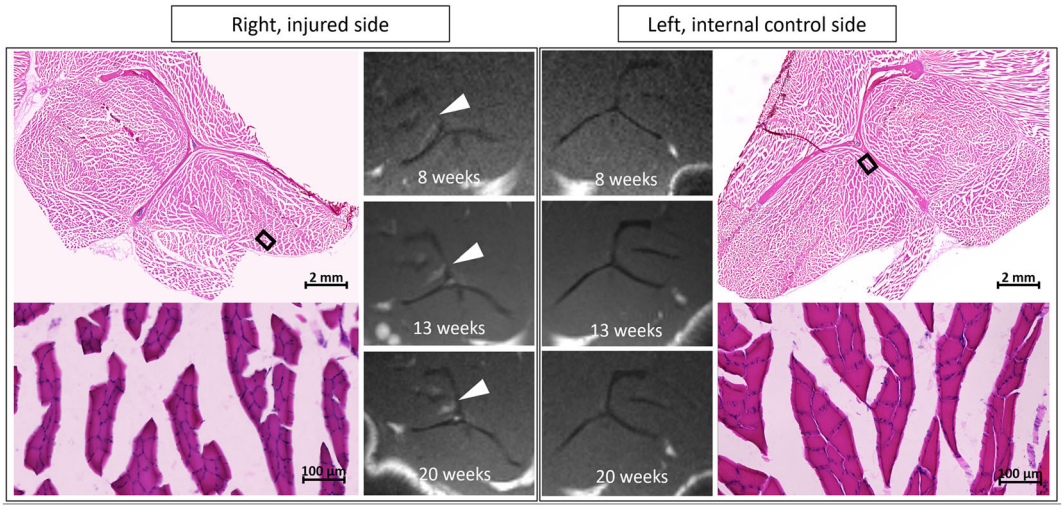

FIGURE 3 Representative muscle changes between sides on conventional magnetic resonance imaging (MRI) and histology. Transverse T1-weighted rapid imaging with refocused echoes (RARE) images of both shoulders demonstrate progressively worsening fatty infiltration in the right infraspinatus (arrowheads), which is Goutallier grade 2 at 20 weeks. Hematoxylin and eosin (H&E)-stained slides at low and higher magnification demonstrate smaller myofiber dimensions on the injured side compared with the internal control side. Black boxes on the low magnification H&E images correspond to the location of the higher magnification regions.

3.3 | Quantitative UTE MRI and histological results

FS was effective in every case. Figure 4 shows representative images of the four quantitative UTE sequences (T1, MT, with and without FS) and representative ROIs. On the non-FS images, foci of high signal intensity are identified on the injured right sides, whereas no perceivable differences between the injured and uninjured sides are evident on the UTE FS images.

Table 1 shows the summary of histological, conventional MRI, and quantitative MRI results. The chronic massive rotator cuff tear model was successful in all rats, as determined by reference-standard histological analysis. Injured myofibers were significantly smaller than the control sides for both the supraspinatus (mean ± SD diameter: 23.0 ± 6.6 vs. 26.4 ± 4.8 µm, $p = 0.04$; mean ± SD perimeter: 109.7 ± 28.5 vs. 126.8 ± 26.1 µm, $p = 0.02$) and infraspinatus (mean ± SD diameter: 20.2 ± 4.4 vs. 25.5 ± 6.2 µm, $p < 0.01$; mean ± SD perimeter: 109.9 ± 24.0 vs. 123.8 ± 25.9 µm, $p = 0.02$) muscles (Figure 3). Similarly, significantly increased extracellular matrix deposition was seen in the injured sides compared with the

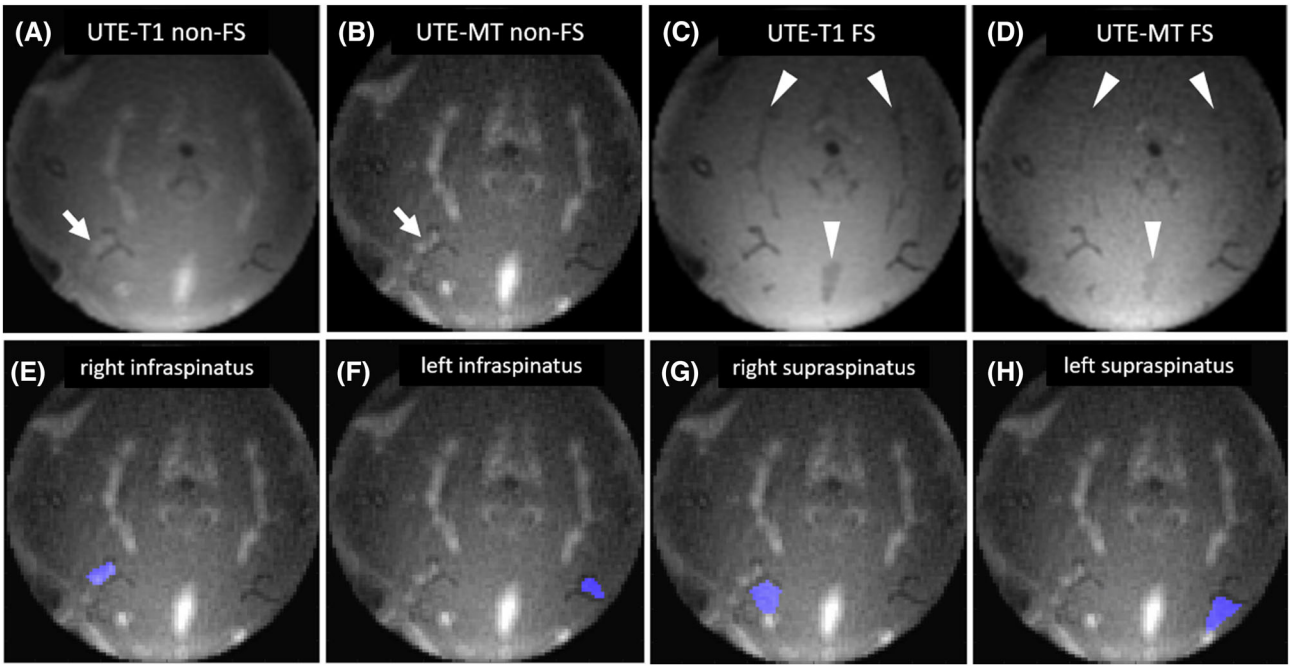

FIGURE 4 Representative source images (A–D) and regions of interest (E–H) used for quantitative UTE magnetic resonance imaging (UTE MRI). Regions of interest over the muscles (purple areas in E–H) were drawn with rapid imaging with refocused echoes (RARE) images as an extra guide (not shown). On the non-FS images, foci of high signal intensity are identified on the injured right sides (arrows in A and B). Fat is effectively suppressed on the FS UTE images, including the intermuscular fat (arrowheads in C and D). FS, fat suppression; UTE-MT, ultrashort echo time magnetization transfer.

TABLE 1 Summary of histological, conventional magnetic resonance imaging (MRI), and quantitative MRI results.

	Supraspinatus			Infraspinatus		
	Injured	Control	*p* value	Injured	Control	*p* value
Myofiber diameter (μm)	23.00 ± 6.61	26.43 ± 4.77	0.04*	20.20 ± 4.39	25.50 ± 6.23	< 0.01*
Myofiber perimeter (μm)	109.66 ± 28.50	126.79 ± 26.11	0.02*	109.91 ± 23.95	123.79 ± 25.93	0.02*
CTF (%)	14.45 ± 3.90	11.29 ± 3.73	0.01*	16.96 ± 5.42	12.48 ± 4.63	< 0.01*
Goutallier grade	1.00 ± 0.60	0.00 ± 0.00	< 0.01*	1.75 ± 0.75	0.33 ± 0.49	< 0.01*
CSA (mm^2)	23.30 ± 5.87	35.38 ± 7.68	< 0.01*	16.47 ± 4.77	27.54 ± 7.07	< 0.01*
T1 non-FS (ms)	902.41 ± 53.69	924.02 ± 48.55	0.11	809.78 ± 83.97	853.67 ± 52.32	0.18
T1 FS (ms)	714.84 ± 41.74	722.85 ± 37.52	0.34	652.25 ± 56.53	667.52 ± 36.35	0.47
MMF non-FS (%)	9.52 ± 0.43	9.45 ± 0.20	0.61	10.38 ± 0.54	10.33 ± 0.18	0.72
MMF FS (%)	9.70 ± 0.26	9.51 ± 0.20	0.04*	10.87 ± 0.79	10.09 ± 0.52	< 0.01*

Note: Paired *t*-test results.
Abbreviations: CSA, cross-sectional area; CTF, connective tissue fraction; FS, fat suppression; MMF, macromolecular fraction.
*Statistically significant result.

control sides for both the supraspinatus (mean ± SD CTF: 14.5% ± 3.9% vs. 11.3% ± 3.7%, $p = 0.01$) and infraspinatus (mean ± SD CTF: 17.0% ± 5.4% vs. 12.5% ± 4.6%, $p < 0.01$) muscles.

As evaluated with quantitative UTE-T1 mapping both with and without FS, mean T1 values were lower for the injured compared with control sides for both supraspinatus and infraspinatus muscles, but the differences did not reach significance (Table 1). Similarly, MMF measured with the UTE-MT non-FS technique did not show statistically significant differences between sides for either the supraspinatus or infraspinatus muscles (Figure 5). However, MMF measured with the UTE-MT FS technique demonstrated statistically significant increases in the injured over the control sides for both supraspinatus (mean ± SD, 9.7% ± 0.3% vs. 9.5% ± 0.2%, $p = 0.04$) and infraspinatus (10.9% ± 0.8% vs. 10.1% ± 0.5%, $p < 0.01$) muscles (Figures 5 and 6).

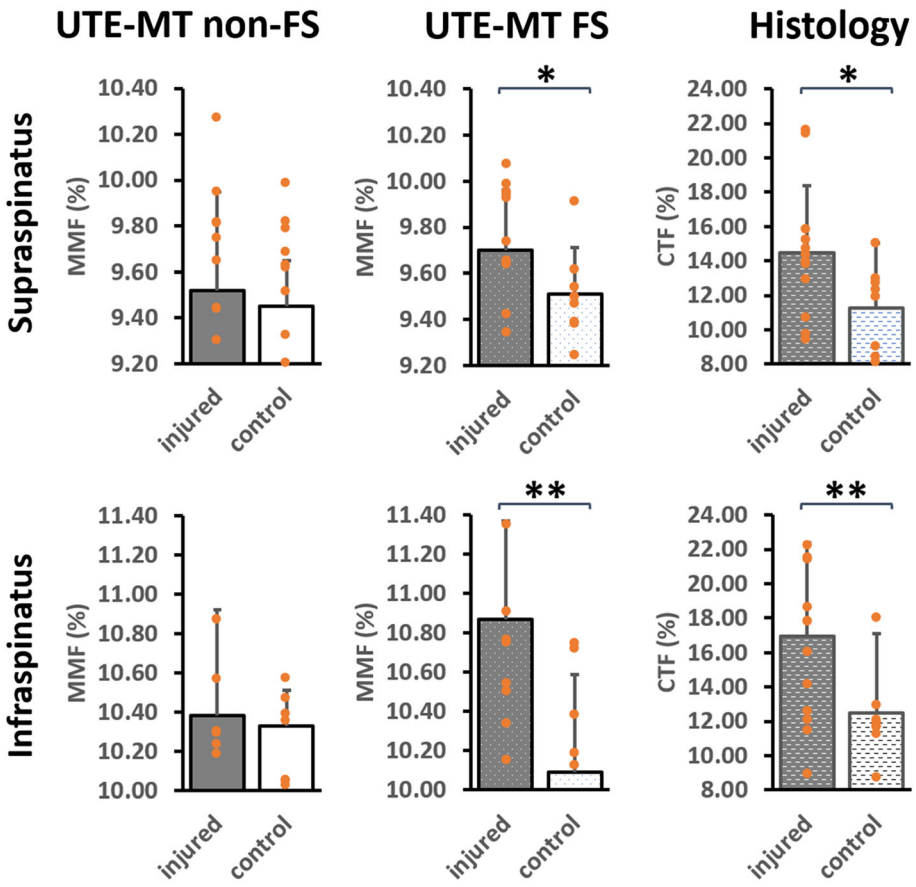

FIGURE 5 Bar graphs overlaid with dot plots of MMF without and with FS as well as histological CTF for bilateral supraspinatus and infraspinatus muscles ($n = 12$ rats). Error bars, mean ± standard deviation. *, $p < 0.05$; **, $p < 0.01$. CTF, connective tissue fraction; FS, fat suppression; MMF, macromolecular fraction; UTE-MT, ultrashort echo times magnetization transfer.

Table 2 shows correlation results between histology and MRI measurements. Notably, MMF assessed with the UTE-MT with FS technique showed statistically significant correlations with CTF for both supraspinatus ($r = 0.46$, $p = 0.03$) and infraspinatus ($r = 0.51$, $p = 0.01$) muscles (Figure 7).

3.4 | Interobserver reliability

Interobserver reliability was good to excellent: 0.98 ($p < 0.01$) for T1 non-FS, 0.97 ($p < 0.01$) for the T1 FS, 0.80 ($p < 0.01$) for MMF non-FS, and 0.78 ($p = 0.01$) for the MMF FS values.

4 | DISCUSSION

In this study we used an established rat model of chronic rotator cuff tearing to evaluate quantitative T1 and MT parameters obtained using UTE imaging techniques with and without FS. We demonstrated that the UTE-MT sequence with FS could be used to show differences in the rotator cuff musculature after injury and that these differences were correlated with the presence of intramuscular fibrosis, confirming our hypothesis. These promising results suggest that a noninvasive imaging technique exists for the evaluation of fibrotic muscle, regardless of the presence of fat.

Of all the models of chronic rotator cuff tearing, the rat is the most commonly utilized animal.[34] We adopted the chronic rotator cuff tear model introduced by Hashimoto et al. by placing an implant over the greater tuberosity to prevent cuff reattachment and scar formation.[24] This is important because the rat has a tremendous capability to heal.[35] The rats in our experiment showed characteristic muscle degeneration, including volume loss (decreased myofiber size and overall muscle CSA), increased fatty infiltration (increased Goutallier grade), and increased fibrosis at

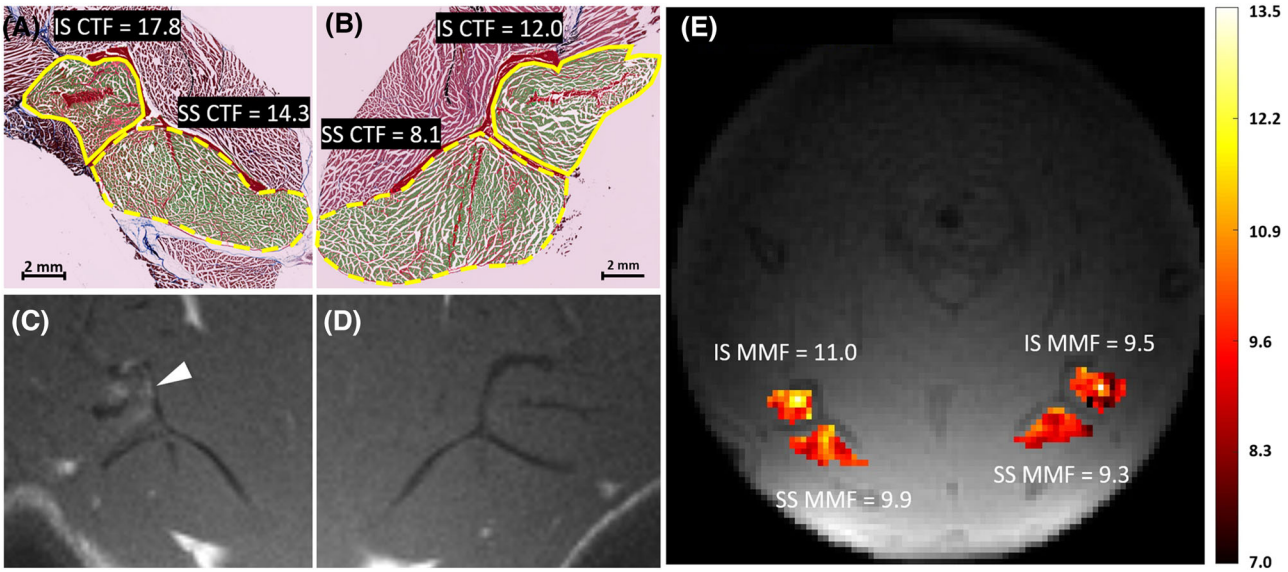

FIGURE 6 Representative correlation between histology and magnetic resonance imaging (MRI) measures. Masson trichrome images of the (A) Injured, and (B) Control sides show the regions of interest (ROIs) used to outline the infraspinatus (solid yellow) and supraspinatus (dashed yellow) muscles. Within the ROIs, collagen-rich extracellular matrix was digitized in red whereas the myofibers were digitized in green. Connective tissue fractions, defined as the area of red divided by the cross-sectional area of the muscle, was higher on the injured sides compared with the control sides. T1-weighted images of the (C) Injured, and (D) Control sides show Goutallier grade 2 fatty infiltration of the right infraspinatus muscle (arrowhead). (E) MMF pixel maps using the ultrashort echo time magnetization transfer fat suppression (UTE-MT FS) technique show higher MMF on the injured compared with the control sides. CTF, connective tissue fraction; IS, infraspinatus; MMF, macromolecular fraction; SS, supraspinatus.

TABLE 2 Summary of correlation results between histology and magnetic resonance imaging (MRI) measurements.

	Supraspinatus			Infraspinatus		
	Myofiber diameter	Myofiber perimeter	CTF	Myofiber diameter	Myofiber perimeter	CTF
Goutallier grade	−0.28, 0.19	−0.28, 0.19	0.40, 0.051	−0.52, < 0.01*	−0.32, 0.13	0.46, 0.02*
CSA	−0.05, 0.83	0.01, 0.98	−0.18, 0.39	0.30, 0.15	0.05, 0.82	−0.52, 0.01*
T1 non-FS	0.10, 0.65	−0.02, 0.94	−0.10, 0.65	0.42, 0.04	0.38, 0.06	−0.14, 0.51
T1 FS	−0.70, 0.75	−0.13, 0.56	−0.10, 0.67	0.39, 0.06	0.35, 0.10	−0.03, 0.90
MMF non-FS	0.17, 0.44	0.13, 0.54	0.07, 0.76	−0.22, 0.30	−0.13, 0.54	0.58, < 0.01*
MMF FS	−0.11, 0.61	0.00, 0.99	0.46, 0.03*	−0.52, 0.01	−0.29, 0.17	0.51, 0.01*

Note: Numbers expressed as: correlation efficient, *p* value.
Abbreviations: CSA, cross-sectional area; CTF, connective tissue fraction; FS, fat suppression; MMF, macromolecular fraction.
*Statistically significant result.

20 weeks postinjury. The infraspinatus muscles demonstrated a greater degree of degeneration than the supraspinatus muscles, similar to the findings of prior investigators.[24,32,36]

Of interest, muscle edema persisted for longer than expected on the conventional MR images. In the initial description of the rat chronic rotator cuff tear model, changes consistent with a chronic tear were observed at 6 weeks.[32] Others have used 12–16 weeks as the chronic postinjury timepoint,[2,24,36,37] with, to the best of our knowledge, the longest timepoint in the rat rotator cuff tear model at 20 weeks postinjury.[12] However, at 20 weeks we noticed that detectable muscular edema persisted in 75% of our animals, suggesting that an even longer postinjury timepoint may be warranted to more closely match the pattern seen in humans. Specifically, muscular edema has been reported to only be present in 4% of chronic, degenerative rotator cuff muscles in humans.[38]

In muscle, the dominant macromolecules include the myofibrillar and collagen proteins,[39] and the MMF obtained from the UTE-MT technique probably reflects the proportion of these proteins relative to the water pool.[14,15] Using animal models, previous authors have shown that the dominant change in pathologic rotator cuff muscle is the increase in collagen content (aside from the fatty infiltration).[4,5,32] Our imaging and histologic results are consistent with these prior studies.

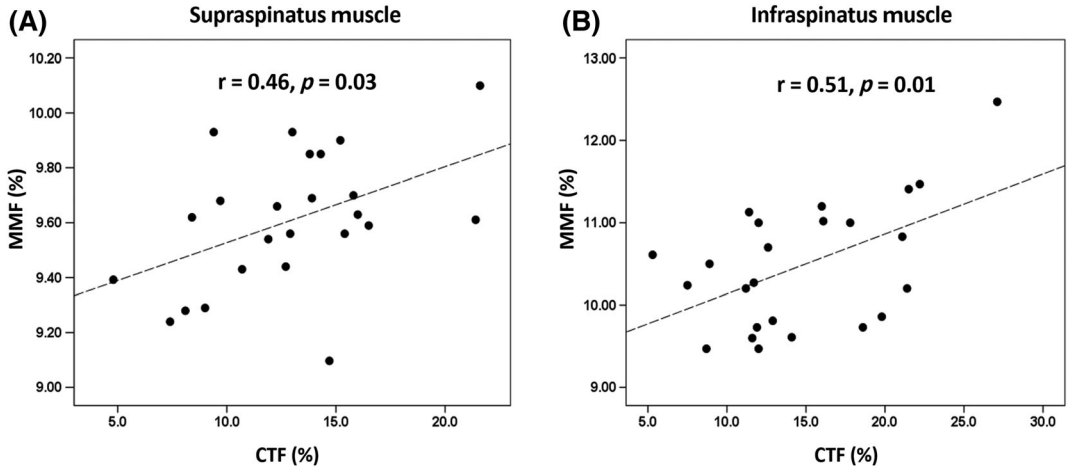

FIGURE 7 Scatterplots showing the relationship of CTF with MMF, obtained with the UTE-MT FS technique, for the (A) Supraspinatus, and (B) Infraspinatus muscles ($n = 24$ each). Dashed lines represent regression lines. CTF, connective tissue fraction; FS, fat suppression; MMF, macromolecular fraction; UTE-MT, ultrashort echo time magnetization transfer.

A range of MMF values in muscles has been reported in the literature. In human lower extremity muscles, values generally range from 6% to 9%,[14,18,40] whereas values between 12% and 17% have been reported in pigs and cattle.[15,41] Thus, the MMF values we obtained in the rat rotator cuff muscles are within the expected range, although are probably underestimated in the injured shoulders due to residual edema. Of note, the MMF differences between injured and control groups would be expected to be even greater if the edema had completely resolved.

Using numerical simulations, Li et al. suggested that the presence of fat causes an underestimation of the macromolecular pool.[17] However, volunteer data from the same group revealed a more complicated relationship because an underestimation or overestimation could be seen,[18] consistent with our results. Jerban et al. recently demonstrated that MMF calculated with measured T1 values were robust for individual voxels containing fat fractions less than 20%, but were more prone to errors when fat fractions exceeded 30%.[42] In fatty muscle degeneration evaluated by pixel-by-pixel analysis, it would be expected that some pixels would be measuring high-fat regions. Li et al. showed that application of FS consistently decreased the variability of the MMF values in muscle.[18] Our results support the measurement of MMF with FS techniques, as this condition appears to most consistently show differences between the abnormal and normal sides, and is also the measure that consistently correlates with the degree of fibrosis across muscles.

Regarding T1 measurements, a range of values in healthy muscle have been reported in the literature. In vivo at 3 T, values ranging from approximately 1000 to 1600 ms have been described in humans, varying with anatomic location, patient age, and imaging technique.[11,20,43,44] Mean T1 values obtained in our study on the control side using the non-FS technique ranged from 854 to 924 ms, which are lower than those obtained by Yang et al. in rat rotator cuff muscle at 3 T (~1200 ms), which may be due to differences in technique because the TE used in our study was 0.026 ms compared with the longer TE of 2.24 ms.[12] UTE detects the bound water component (with shorter T1 values) in addition to the free water component, and thus lower overall mean T1 values are expected.[45] With the application of FS, T1 values consistently decreased in our study, similar to what others have reported.[20] While the exclusion of T1-shortening fat may be expected to increase the effective T1 value, particularly for the injured muscles, the MT effects from the off-resonance fat saturation pulse dominate,[20,46–48] resulting in a decrease in effective T1.

T1 mapping after the intravenous administration of a gadolinium-based contrast agent (GBCA) has been used to evaluate cardiac and skeletal muscle. In cardiomyopathy patients with endomyocardial biopsy samples, Sibley et al. previously demonstrated that T1 time and histologic fibrosis were inversely correlated ($r = -0.57$).[29] More recently, Marty et al. used an MR fingerprinting sequence with water and fat separation before and after the intravenous administration of a GBCA in conjunction with serum hematocrit values to calculate extracellular volume (ECV) fraction, which is another candidate variable to characterize muscle tissue microstructure.[49] Patients with Becker muscular dystrophy were compared with controls and the authors found that ECV fraction was higher in the patients, even those with normal muscle fat fraction.[49] The authors hypothesized that muscle ECV expansion reflects a combination of collagen deposition, extracellular edema, and dying myocytes. Future studies comparing ECV and UTE-MT measures are warranted.

Our study has several limitations. First is the use of an animal model, which has some disadvantages.[34] Rats have a strong self-healing capability, which was the rationale for the silicone implant in our study. Despite possessing the closest resemblance to the anatomic structure of the human shoulder out of 33 animals,[50] there remain significant differences in muscle degeneration after chronic rotator cuff injury compared with humans. For instance, even at the longest postoperative time interval used in the rat cuff model to date (20 weeks), muscle edema persisted in the majority of our cases. Evaluation of human rotator cuff muscles in vivo using heavily accelerated MRI techniques should be performed and

are planned as future work. Second, measurements of fibrosis are imperfect. We utilized histology as a reference standard to maximize anatomic colocalization between modalities. However, some artifacts are unavoidable with this technique. Biochemical analysis may yield more precise quantification, but the opportunity for anatomic colocalization with MRI slices would not be possible. Third, our methodology did not account for myotendinous retraction, which has been reported to cause discrepancies in the assessment of muscle degeneration.[51] However, in both clinical practice and research settings, reliance on osseous landmarks for slice selection is the most commonly utilized method. Fourth, although the correlation coefficients between MMF values measured with the UTE-MT FS sequence and CTF were statistically significant, they are only moderate in strength. The viability of this technique to draw meaningful distinctions in individual human subjects remains to be determined in future work. Finally, intramuscular tendons were not excluded in our study because precise segmentation of tendon from peritendinous fibrosis in the muscle could not be accurately made on MRI. However, intramuscular tendons were included on all evaluations, including conventional MRI, quantitative MRI, and histological measurements. Although the collagen-rich extracellular matrix of tendons would lead to an overestimation of both muscle MMF on quantitative MRI and CTF/fibrosis on histology, the correlation results between the measures would not be expected to be adversely affected.

In conclusion, the UTE-MT with FS technique can be used to differentiate between injured and control rotator cuff muscles. Both fatty infiltration and fibrosis occur in rotator cuff muscle degeneration, and the UTE-MT with FS technique may be helpful to evaluate the fibrosis component, independent from the fatty infiltration process.

ACKNOWLEDGMENTS

The authors acknowledge grant support from the Veterans Affairs Clinical Science and Biomedical Laboratory R&D (I01CX001388, I01BX005952, and I01CX000625) and National Institutes of Health (R01AR068987, R01AR062581, R01AR075825, K01AR080257, R01AR079484, and R21AR075851).

CONFLICT OF INTEREST STATEMENT

The authors have no conflicts of interest to declare.

REFERENCES

1. Kramer EJ, Bodendorfer BM, Laron D, et al. Evaluation of cartilage degeneration in a rat model of rotator cuff tear arthropathy. *J Shoulder Elbow Surg*. 2013;22(12):1702-1709. doi:10.1016/j.jse.2013.03.014
2. Gimbel JA, Mehta S, Van Kleunen JP, Williams GR, Soslowsky LJ. The tension required at repair to reappose the supraspinatus tendon to bone rapidly increases after injury. *Clin Orthop Relat Res*. 2004;426:258-265. doi:10.1097/01.blo.0000136831.17696.80
3. Kuzel BR, Grindel S, Papandrea R, Ziegler D. Fatty infiltration and rotator cuff atrophy. *J Am Acad Orthop Surg*. 2013;21(10):613-623. doi:10.5435/JAAOS-21-10-613
4. Meyer DC, Hoppeler H, von Rechenberg B, Gerber C. A pathomechanical concept explains muscle loss and fatty muscular changes following surgical tendon release. *J Orthop Res*. 2004;22(5):1004-1007. doi:10.1016/j.orthres.2004.02.009
5. Sato EJ, Killian ML, Choi AJ, et al. Skeletal muscle fibrosis and stiffness increase after rotator cuff tendon injury and neuromuscular compromise in a rat model. *J Orthop Res*. 2014;32(9):1111-1116. doi:10.1002/jor.22646
6. Saveh Shemshaki N, Kan HM, Barajaa M, et al. Muscle degeneration in chronic massive rotator cuff tears of the shoulder: addressing the real problem using a graphene matrix. *Proc Natl Acad Sci U S A*. 2022;119(33):e2208106119. doi:10.1073/pnas.2208106119
7. Slabaugh MA, Friel NA, Karas V, Romeo AA, Verma NN, Cole BJ. Interobserver and intraobserver reliability of the Goutallier classification using magnetic resonance imaging: proposal of a simplified classification system to increase reliability. *Am J Sports Med*. 2012;40(8):1728-1734. doi:10.1177/0363546512452714
8. Huang Y, Majumdar S, Genant HK, et al. Quantitative MR relaxometry study of muscle composition and function in Duchenne muscular dystrophy. *J Magn Reson Imaging*. 1994;4(1):59-64. doi:10.1002/jmri.1880040113
9. Park JH, Olsen NJ, King L Jr, et al. Use of magnetic resonance imaging and P-31 magnetic resonance spectroscopy to detect and quantify muscle dysfunction in the amyopathic and myopathic variants of dermatomyositis. *Arthritis Rheum*. 1995;38(1):68-77. doi:10.1002/art.1780380111
10. Marty B, Coppa B, Carlier PG. Monitoring skeletal muscle chronic fatty degenerations with fast T1-mapping. *Eur Radiol*. 2018;28(11):4662-4668. doi:10.1007/s00330-018-5433-z
11. Marty B, Carlier PG. Physiological and pathological skeletal muscle T1 changes quantified using a fast inversion-recovery radial NMR imaging sequence. *Sci Rep*. 2019;9(1):6852. doi:10.1038/s41598-019-43398-x
12. Yang Y, Qiu L, Gu X, et al. Monitoring rotator cuff muscle fatty infiltration progression by magnetic resonance imaging T1 mapping: correlation with direct evaluation findings in rats. *Am J Sports Med*. 2022;50(4):1078-1087. doi:10.1177/03635465211069976
13. McDaniel JD, Ulmer JL, Prost RW, et al. Magnetization transfer imaging of skeletal muscle in autosomal recessive limb girdle muscular dystrophy. *J Comput Assist Tomogr*. 1999;23(4):609-614. doi:10.1097/00004728-199907000-00023
14. Sinclair CD, Samson RS, Thomas DL, et al. Quantitative magnetization transfer in in vivo healthy human skeletal muscle at 3 T. *Magn Reson Med*. 2010;64(6):1739-1748. doi:10.1002/mrm.22562
15. Bajd F, Skrlep M, Candek-Potokar M, Vidmar J, Sersa I. Application of quantitative magnetization transfer magnetic resonance imaging for characterization of dry-cured hams. *Meat Sci*. 2016;122:109-118. doi:10.1016/j.meatsci.2016.08.001
16. Romero IO, Sinha U. Magnetization transfer saturation imaging of human calf muscle: reproducibility and sensitivity to regional and sex differences. *J Magn Reson Imaging*. 2019;50(4):1227-1237. doi:10.1002/jmri.26694

17. Li K, Dortch RD, Kroop SF, et al. A rapid approach for quantitative magnetization transfer imaging in thigh muscles using the pulsed saturation method. *Magn Reson Imaging*. 2015;33(6):709-717. doi:10.1016/j.mri.2015.03.003
18. Li K, Dortch RD, Welch EB, et al. Multi-parametric MRI characterization of healthy human thigh muscles at 3.0 T—relaxation, magnetization transfer, fat/water, and diffusion tensor imaging. *NMR Biomed*. 2014;27(9):1070-1084. doi:10.1002/nbm.3159
19. Nuñez-Peralta C, Montesinos P, Alonso-Jiménez A, et al. Magnetization transfer ratio in lower limbs of late onset Pompe patients correlates with intramuscular fat fraction and muscle function tests. *Front Neurol*. 2021;12:634766. doi:10.3389/fneur.2021.634766
20. White JC, Sinha S, Sinha U. Spin lattice (T1) and magnetization transfer saturation (MT_{sat}) imaging to monitor age-related differences in skeletal muscle tissue. *Diagnostics*. 2022;12(3):584. doi:10.3390/diagnostics12030584
21. Iijima Y, Matsuki K, Hoshika S, et al. Differences in fatty degeneration of rotator cuff muscles at different sites, as quantified by T2 mapping. *J Orthop Sci*. 2017;22(2):281-284. doi:10.1016/j.jos.2016.11.016
22. de Mello R, Ma Y, Ji Y, Du J, Chang EY. Quantitative MRI musculoskeletal techniques: an update. *Am J Roentgenol*. 2019;213(3):524-533. doi:10.2214/AJR.19.21143
23. Guo T, Ma YJ, High RA, et al. Assessment of an in vitro model of rotator cuff degeneration using quantitative magnetic resonance and ultrasound imaging with biochemical and histological correlation. *Eur J Radiol*. 2019;121:108706. doi:10.1016/j.ejrad.2019.108706
24. Hashimoto E, Ochiai N, Kenmoku T, et al. Macroscopic and histologic evaluation of a rat model of chronic rotator cuff tear. *J Shoulder Elbow Surg*. 2016;25(12):2025-2033. doi:10.1016/j.jse.2016.04.024
25. Ashir A, Lombardi A, Jerban S, Ma Y, Du J, Chang EY. Magnetic resonance imaging of the shoulder. *Pol J Radiol*. 2020;85:e420-e439. doi:10.5114/pjr.2020.98394
26. Fuchs B, Weishaupt D, Zanetti M, Hodler J, Gerber C. Fatty degeneration of the muscles of the rotator cuff: assessment by computed tomography versus magnetic resonance imaging. *J Shoulder Elbow Surg*. 1999;8(6):599-605. doi:10.1016/s1058-2746(99)90097-6
27. Somerson JS, Hsu JE, Gorbaty JD, Gee AO. Classifications in brief: Goutallier classification of fatty infiltration of the rotator cuff musculature. *Clin Orthop Relat Res*. 2016;474(5):1328-1332. doi:10.1007/s11999-015-4630-1
28. Ma YJ, Chang EY, Carl M, Du J. Quantitative magnetization transfer ultrashort echo time imaging using a time-efficient 3D multispoke Cones sequence. *Magn Reson Med*. 2018;79(2):692-700. doi:10.1002/mrm.26716
29. Sibley CT, Noureldin RA, Gai N, et al. T1 mapping in cardiomyopathy at cardiac MR: comparison with endomyocardial biopsy. *Radiology*. 2012;265(3):724-732. doi:10.1148/radiol.12112721
30. Sevivas N, Serra SC, Portugal R, et al. Animal model for chronic massive rotator cuff tear: behavioural and histologic analysis. *Knee Surg Sports Traumatol Arthrosc*. 2015;23(2):608-618. doi:10.1007/s00167-014-3441-3
31. Sasaki Y, Ochiai N, Nakajima A, et al. Histological analysis and biomechanical evaluation of fatty infiltration after rotator cuff tear and suprascapular nerve injury in a rat model. *J Orthop Sci*. 2018;23(5):834-841. doi:10.1016/j.jos.2018.04.004
32. Liu X, Manzano G, Kim HT, Feeley BT. A rat model of massive rotator cuff tears. *J Orthop Res*. 2011;29(4):588-595. doi:10.1002/jor.21266
33. Koo TK, Li MY. A guideline of selecting and reporting intraclass correlation coefficients for reliability research. *J Chiropr Med*. 2016;15(2):155-163. doi:10.1016/j.jcm.2016.02.012
34. Zhao W, Yang J, Kang Y, et al. Animal models of rotator cuff injury and repair: a systematic review. *Tissue Eng Part B Rev*. 2022;28(6):1258-1273. doi:10.1089/ten.TEB.2022.0034
35. Buchmann S, Walz L, Sandmann GH, et al. Rotator cuff changes in a full thickness tear rat model: verification of the optimal time interval until reconstruction for comparison to the healing process of chronic lesions in humans. *Arch Orthop Trauma Surg*. 2011;131(3):429-435. doi:10.1007/s00402-010-1246-5
36. Kim HM, Galatz LM, Lim C, Havlioglu N, Thomopoulos S. The effect of tear size and nerve injury on rotator cuff muscle fatty degeneration in a rodent animal model. *J Shoulder Elbow Surg*. 2012;21(7):847-858. doi:10.1016/j.jse.2011.05.004
37. Mannava S, Plate JF, Whitlock PW, et al. Evaluation of in vivo rotator cuff muscle function after acute and chronic detachment of the supraspinatus tendon: an experimental study in an animal model. *J Bone Joint Surg Am*. 2011;93(18):1702-1711. doi:10.2106/JBJS.J.00184
38. Loew M, Magosch P, Lichtenberg S, Habermeyer P, Porschke F. How to discriminate between acute traumatic and chronic degenerative rotator cuff lesions: an analysis of specific criteria on radiography and magnetic resonance imaging. *J Shoulder Elbow Surg*. 2015;24(11):1685-1693. doi:10.1016/j.jse.2015.06.005
39. Haus JM, Carrithers JA, Carroll CC, Tesch PA, Trappe TA. Contractile and connective tissue protein content of human skeletal muscle: effects of 35 and 90 days of simulated microgravity and exercise countermeasures. *Am J Physiol Regul Integr Comp Physiol*. 2007;293(4):R1722-R1727. doi:10.1152/ajpregu.00292.2007
40. Chen Y, Li L, Le N, Chang EY, Huang W, Ma YJ. On the fat saturation effect in quantitative ultrashort TE MR imaging. *Magn Reson Med*. 2022;87(5):2388-2397. doi:10.1002/mrm.29149
41. Sled JG, Pike GB. Quantitative imaging of magnetization transfer exchange and relaxation properties in vivo using MRI. *Magn Reson Med*. 2001;46(5):923-931. doi:10.1002/mrm.1278
42. Jerban S, Ma Y, Tang Q, et al. Robust assessment of macromolecular fraction (MMF) in muscle with differing fat fraction using ultrashort echo time (UTE) magnetization transfer modeling with measured T1. *Diagnostics*. 2023;13(5):876. doi:10.3390/diagnostics13050876
43. Gold GE, Han E, Stainsby J, Wright G, Brittain J, Beaulieu C. Musculoskeletal MRI at 3.0 T: relaxation times and image contrast. *Am J Roentgenol*. 2004;183(2):343-351. doi:10.2214/ajr.183.2.1830343
44. Morrow JM, Sinclair CD, Fischmann A, et al. Reproducibility, and age, body-weight and gender dependency of candidate skeletal muscle MRI outcome measures in healthy volunteers. *Eur Radiol*. 2014;24(7):1610-1620. doi:10.1007/s00330-014-3145-6
45. Mahar R, Batool S, Badar F, Xia Y. Quantitative measurement of T2, T1rho and T1 relaxation times in articular cartilage and cartilage-bone interface by SE and UTE imaging at microscopic resolution. *J Magn Reson*. 2018;297:76-85. doi:10.1016/j.jmr.2018.10.008
46. Henkelman RM, Stanisz GJ, Graham SJ. Magnetization transfer in MRI: a review. *NMR Biomed*. 2001;14(2):57-64. doi:10.1002/nbm.683
47. Robson MD, Piechnik SK, Tunnicliffe EM, Neubauer S. T1 measurements in the human myocardium: the effects of magnetization transfer on the SASHA and MOLLI sequences. *Magn Reson Med*. 2013;70(3):664-670. doi:10.1002/mrm.24867
48. Kellman P, Hansen MS. T1-mapping in the heart: accuracy and precision. *J Cardiovasc Magn Reson*. 2014;16(1):2. doi:10.1186/1532-429X-16-2

49. Marty B, Baudin PY, de Almeida C, et al. Assessment of extracellular volume fraction in Becker muscular dystrophy by using MR fingerprinting. *Radiology*. 2023;307(3):e221115. doi:10.1148/radiol.221115
50. Soslowsky LJ, Carpenter JE, DeBano CM, Banerji I, Moalli MR. Development and use of an animal model for investigations on rotator cuff disease. *J Shoulder Elbow Surg*. 1996;5(5):383-392. doi:10.1016/s1058-2746(96)80070-x
51. Yoo HJ, Choi JY, Hong SH, Kim EJ, Kim SH. Quantifying rotator cuff atrophy and fatty degeneration at the supraspinatus origin in the scapular fossa. *Knee Surg Sports Traumatol Arthrosc*. 2015;23(2):399-407. doi:10.1007/s00167-014-2992-7

How to cite this article: Chang EY, Suprana A, Tang Q, et al. Rotator cuff muscle fibrosis can be assessed using ultrashort echo time magnetization transfer MRI with fat suppression. *NMR in Biomedicine*. 2024;37(2):e5058. doi:10.1002/nbm.5058